environmental sciences proceedings

MDPI

Proceedings

Optical Properties and Direct Radiative Effects of Aerosol Species at the Global Scale Based on the Synergistic Use of MERRA-2 Optical Properties and the FORTH Radiative Transfer Model †

Marios-Bruno Korras-Carraca [1,2,*], Antonis Gkikas [3], Arlindo M. Da Silva [4], Christos Matsoukas [2], Nikolaos Hatzianastassiou [1,*] and Ilias Vardavas [5]

[1] Laboratory of Meteorology, Department of Physics, University of Ioannina, 451 10 Ioannina, Greece
[2] Department of Environment, University of the Aegean, 811 00 Mytilene, Greece; matsoukas@aegean.gr
[3] Institute for Astronomy, Astrophysics, Space Applications and Remote Sensing (IAASARS), National Observatory of Athens, 118 51 Athens, Greece; agkikas@noa.gr
[4] NASA/GSFC, Greenbelt, MD 20771, USA; arlindo.m.dasilva@nasa.gov
[5] Department of Physics, University of Crete, 700 13 Heraklion, Greece; vardavas@uoc.gr
* Correspondence: koras@env.aegean.gr (M.-B.K.-C.); nhatzian@uoi.gr (N.H.)
† Presented at the 3rd International Electronic Conference on Atmospheric Sciences, 16–30 November 2020; Available online: https://ecas2020.sciforum.net/.

Abstract: The overarching goal of the current study is to quantify the aerosol-induced clear-sky direct radiative effects (DREs) within the Earth-atmosphere system at the global scale and for the 40-year period 1980–2019. To this aim, the MERRA-2 aerosol radiative properties, along with meteorological fields and surface albedo, are used as inputs to the Foundation for Research and Technology-Hellas (FORTH) radiative transfer model (RTM). Our preliminary results, representative for the year 2015, reveal strong surface radiative cooling (down to −45 Wm^{-2}) over areas where high aerosol loadings and absorbing particles (i.e., dust and biomass burning) dominate. This reduction of the incoming solar radiation in the aforementioned regions is largely attributed to its absorption by the overlying suspended particles resulting in atmospheric warming reaching up to 40 Wm^{-2}. At the top of the atmosphere (TOA), negative DREs (planetary cooling) are computed worldwide (down to −20 Wm^{-2}) with few exceptions over bright surfaces (warming up to 5 Wm^{-2}). Finally, the strong variations between the obtained DREs of different aerosol species (dust, sea salt, sulfate, and organic/black carbon) as well as between hemispheres and surface types (i.e., land vs. ocean) are also discussed.

Keywords: aerosols; aerosol direct radiative effects; global aerosol reanalysis

Citation: Korras-Carraca, M.-B.; Gkikas, A.; Da Silva, A.M.; Matsoukas, C.; Hatzianastassiou, N.; Vardavas, I. Optical Properties and Direct Radiative Effects of Aerosol Species at the Global Scale Based on the Synergistic Use of MERRA-2 Optical Properties and the FORTH Radiative Transfer Model. *Environ. Sci. Proc.* **2021**, *4*, 4. https://doi.org/10.3390/ ecas2020-08151

Academic Editor: Anthony R. Lupo

Published: 13 November 2020

1. Introduction

Aerosols, among other atmospheric constituents, through their interaction with radiation, exert a perturbation on the Earth-atmosphere system energy budget, thus playing a key role in the current and future climate. Originating from natural and anthropogenic sources worldwide, the microphysical and optical properties of the suspended particles, which determine the aerosol-radiation interactions, reveal a remarkable variability both in space and time. Moreover, the vertical structure of aerosol layers, as well as the underlying surface properties, impose an additional complexity in the assessment of the relevant radiative effects under clear-sky conditions. Quantifying the aerosol radiative effects at global and regional scales, requires accurate speciation of tropospheric and stratospheric aerosol types, as well as an optimum characterization of

their key radiative properties, namely the aerosol optical depth (AOD), single scattering albedo (SSA) and asymmetry parameter (g). Such challenging tasks can be fulfilled either by observations or modeling techniques, which are both characterized by specific advantages and drawbacks. A comprehensive analysis in aerosol-radiation studies requires the estimation of radiative effects per each aerosol type and their contribution to the total perturbation at long-term (i.e., decadal) scales aiming at reducing the current uncertainty levels reported by the Intergovernmental Panel of Climate Change (IPCC) [1].

In this study, we use the full dataset of MERRA-2 reanalysis aerosol optical properties [2,3], spanning over four decades (1980–2019our), along with a radiative transfer model (RTM) in order to investigate the spatio-temporal distribution of the clear-sky direct radiative effects (DREs) per aerosol type as well as for the total aerosol load. As a demonstration of our analysis, we present here preliminary results, referring to the year 2015, for the perturbed radiation fields at the top of the atmosphere (TOA), within the atmosphere, and at the surface.

2. Methods

The aerosol DREs are computed using the deterministic spectral radiation transfer model FORTH [4], developed from a radiative-convective model [5]. The model computations are performed on a monthly 0.5° × 0.625° horizontal resolution (the original MERRA-2 resolution). The monochromatic radiative flux transfer equations are solved in 118 wavelengths between 0.20 and 1 μm and 10 spectral intervals between 1 and 10 μm, assuming an absorbing/multiple-scattering atmosphere and using the Delta–Eddington method.

In order to calculate the aerosol DRE, the model requires their vertically and spectrally resolved optical properties (i.e., AOD, SSA, and g). However, MERRA-2 does not directly provide such data. Therefore, we computed them based on 3-hourly vertically resolved instantaneous aerosol mixing ratios and relative humidity data (both included in the MERRA-2 reanalysis and provided in 72 vertical layers) and look-up tables that provide the scattering and absorption efficiencies per aerosol type, aerosol size bin, relative humidity, and 25 wavelengths. Apart from aerosols, all remaining RTM-required input data (surface albedo, specific humidity, and ozone concentration) were also taken from MERRA-2.

The aerosol DREs were computed at the Earth's surface, within the atmosphere, and at the top of the atmosphere (TOA) as

$$DRE_x = F_{aer} - F_{no\text{-}aer\text{-}x}, \quad (1)$$

where x corresponds to the aerosol type (sulfate, sea salt, dust, organic carbon, black carbon, and total), F_{aer} is the net downward (downward minus upward) radiative flux obtained running the RTM with all aerosol types, and $F_{no\text{-}aer\text{-}x}$ is the corresponding flux computed with the RTM without considering a particular aerosol type x (in the case of x = total, $F_{no\text{-}aer\text{-}x}$ corresponds to an atmosphere without any aerosols).

3. Results and Discussion

3.1. Aerosol Optical Properties for the Year 2015

We begin this section with a brief presentation of the main patterns of the geographic variation of the MERRA-2 AOD and SSA. As shown in Figure 1a, significant spatial variability of the AOD is evident. The highest aerosol load (up to 0.77, on a mean annual level) is observed in east China. In this region, according to MERRA-2 (results not shown here), the aerosol load is dominated by sulfate particles but also by significant loads of carbonaceous (organic and black carbon) particles. Equally high aerosol load (AOD up to 0.73) is observed in North Africa, especially above the dust-dominated southern and southwestern parts of the Sahara Desert and the western Sub-Sahel. Over the latter region, besides the advected desert dust, there is also a strong presence of carbonaceous particles

(organic and black carbon) originating from biomass burning taking place during winter (dry season). High aerosol load is observed over most arid and semi-arid regions of the planet, with AOD reaching 0.50 over the Arabian Peninsula and 0.45 over the Taklamakan desert. Over the Indian subcontinent, the presence of significant aerosol sources (both natural, such as the Thar Desert, and anthropogenic) results in AOD values that are generally larger than 0.30 and reach 0.53 over the Indo-Gangetic Plain. High aerosol loads are also evident over regions with frequent seasonal biomass burning and, therefore, a strong presence of carbonaceous particles. Thus, AOD values reach up 0.46 over central-southern Africa, 0.34 over maritime Southeast Asia, 0.25 over South America, and 0.17 over Northwestern America. On the other hand, the aerosol load is low (AOD less than 0.1) above most oceanic regions. However, in the case of long-range transport of continental particles above oceanic regions, the aerosol load may be very high. Such a characteristic case is the Saharan dust and biomass burning outflows to the tropical and subtropical North Atlantic Ocean and the Gulf of Guinea, resulting in AOD as high as 0.40. Other oceanic regions with relatively high aerosol load are the tropical South Atlantic, where mainly carbonaceous particles are transported from the African continent, and the North Indian Ocean (transportation of both natural and anthropogenic particles from the Indian subcontinent and the Arabian Peninsula).

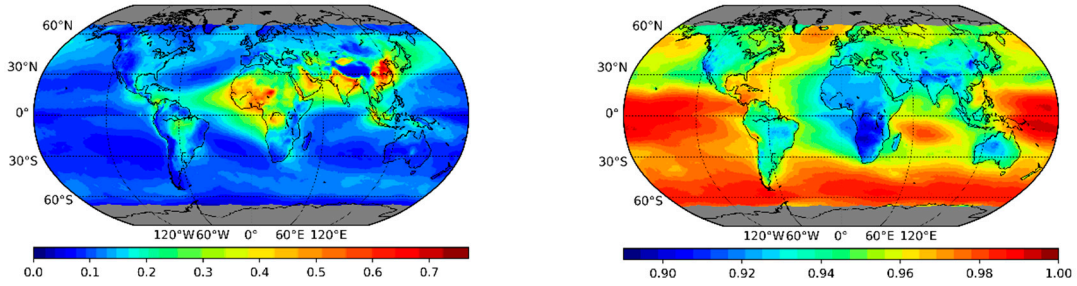

(**a**) (**b**)

Figure 1. Mean annual (2015) global distribution of MERRA-2 optical properties for the total aerosol load at 550 nm: (**a**) aerosol optical depth; (**b**) single scattering albedo.

The aerosol SSA values (Figure 1b) range between 0.89 and 1.0. The lowest values (deep blue colors) are observed over regions where the aerosol load is dominated by biomass burning aerosols, including the strong absorptive black carbon particles. The most characteristic region with low SSA values (generally lower than 0.92) is Central and Southern Africa. Relatively low SSA is also observed above eastern and southern Asia, the Sahara Desert, western United States, western Europe, and the tropical Atlantic Ocean. On the other hand, over most remote oceanic regions, the SSA is high due to the dominance of non-absorbing sea salt particles.

3.2. Aerosol Radiative Effects for the Year 2015

The mean annual geographical distribution of the aerosol effects on the net shortwave flux at the Earth's surface (hereafter $DRE_{surfnet}$), within the atmosphere (DRE_{atm}), and at TOA (DRE_{TOA}) for the year 2015 is presented in Figure 2.

At the Earth's surface (Figure 2a), aerosol causes a cooling effect (negative $DRE_{surfnet}$). This cooling is associated with the reduction of the downwelling solar radiation due to scattering and absorption by aerosol particles and is more pronounced over regions with a high aerosol load. More specifically, the strongest cooling effect (up to −45 Wm^{-2}) is observed over east China, which is characterized by high loads of strongly scattering sulfate particles. A strong cooling effect is also evident over North Africa (strong presence of desert dust and carbonaceous particles), with $DRE_{surfnet}$ ranging between −15 and −35 Wm^{-2} over most of the Sahara Desert and reaching −40 Wm^{-2} in the Sub-Sahel (Niger delta

region). A pronounced cooling effect is observed over Central Africa ($DRE_{surfnet}$ −20 to −38 Wm^{-2}), the Indo-Gangetic Plain (cooling up to 40 Wm^{-2} locally), and the Arabian Peninsula as well as above neighboring oceanic regions where aerosols are transported from the former source areas.

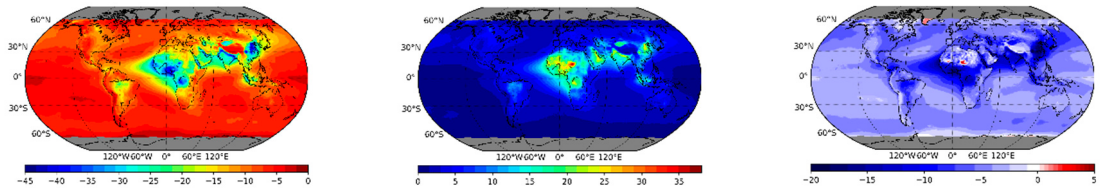

(**a**) (**b**) (**c**)

Figure 2. Mean annual (2015) global distribution of aerosol direct radiative effect (Wm^{-2}): (**a**) at the Earth's surface; (**b**) within the atmosphere; (**c**) at the top of the atmosphere (TOA).

The aerosol effect within the atmosphere (hereafter DRE_{atm}) is presented in Figure 2b. It is evident that aerosols cause a heating of the atmosphere (by increasing the atmospheric absorption). This heating effect is stronger in regions with high aerosol loads and absorbing particles, characterized by relatively low SSA. Although DRE_{atm} has an opposite sign to that of $DRE_{surfnet}$, their geographic distributions are similar. The atmospheric heating is especially pronounced above North Africa (DRE_{atm} up to 38 Wm^{-2} over the southern Saharan Desert). A relatively strong aerosol heating is also observed above the Arabian Peninsula (up to 24 Wm^{-2}). Over the biomass burning dominated Central Africa, and the highly populated Southern and Eastern Asia, aerosols cause atmospheric heating equal to 20–24 Wm^{-2} locally.

The geographical distribution of the aerosol effect at the top of the atmosphere (hereafter DRE_{TOA}) is shown in Figure 2c. The values of DRE_{TOA} range between −20 to 5 Wm^{-2}. Negative values indicate decreasing net incoming solar radiation (i.e., planetary cooling due to increased backscattered solar radiation to space), while positive values indicate planetary warming. It is evident that aerosols cause a cooling effect above most parts of the globe. This planetary cooling is much more pronounced (DRE_{TOA} ranging between −10 to −20 Wm^{-2}) over the Sahel and Sub-Sahel, Central Africa, the Indian subcontinent, and Eastern China, namely over regions characterized by a high aerosol load of both natural and anthropogenic origin. Strong planetary cooling is also observed above oceanic regions where continental aerosols are advected (such as the tropical Atlantic Ocean and the northern Indian Ocean). Note that over the Arabian Peninsula and the Sahara Desert, DRE_{TOA} is relatively low, despite the presence of high loads of desert dust. In some parts of the Sahara Desert, there is even a planetary warming effect (up to 4–5 Wm^{-2}, locally). These arid regions are characterized by strong surface albedo (greater than 0.25), resulting in multiple scattering between relatively absorbing desert dust particles and the ground [6,7]. Therefore, there is a near-cancellation of the surface cooling by an equally large atmospheric warming over most parts of these regions. The aerosol planetary heating effect is observed over the parts of Sahara with the highest surface albedo, highlighting the importance of this parameter for the determination of the sign of DRE_{TOA}. The small planetary heating observed over the ice-covered southern Greenland can also be explained by the very high surface albedo therein.

The globally and hemispherically averaged values of the aerosol DREs, as well as the DREs averaged over global land and ocean areas, are presented in Table 1. Under clear-sky conditions, aerosols cause a cooling effect of −8.73 Wm^{-2} at the Earth's surface and a warming of the atmosphere equal to 3.94 Wm^{-2}. The surface cooling is larger in magnitude than the atmospheric warming effect; therefore, aerosol particles cause a planetary cooling effect at TOA of −4.79 Wm^{-2}. The aerosol DREs exhibit differences in their magnitude between land and oceans as well as between the two hemispheres. The aerosol effects are larger over land than over ocean and over the Northern Hemisphere compared to the

Southern. These differences are more pronounced for the DRE_{atm}, and they are related to the presence of stronger and more absorbing aerosols over the Northern Hemisphere and global land areas.

Table 1. Annual averaged total aerosol direct radiative effects (DREs) (in Wm^{-2}) for 2015 over: the globe, the Northern and Southern Hemispheres, global land, and global ocean areas. The corresponding averages for aerosol optical depth (AOD) and single scattering albedo (SSA) at 550 nm are shown in the last columns.

	DRE_{TOA}	DRE_{atm}	$DRE_{surfnet}$	AOD	SSA
Global	−4.79	3.94	−8.73	0.137	0.957
Land	−5.33	6.66	−11.98	0.172	0.938
Ocean	−4.55	2.72	−7.27	0.121	0.965
N. Hemisphere	−5.64	5.41	−11.05	0.171	0.950
S. Hemisphere	−3.96	2.50	−6.46	0.104	0.963

In Tables 2–6, we provide the averaged DREs of each aerosol particle type (i.e., sulfate, dust, sea salt, organic carbon, and black carbon) separately in order to provide some insight into their contribution to the total aerosol effect. From these results, large differences between the DREs of different particle types are evident. More specifically, the strongest cooling effect on the Earth's surface is caused by desert dust (−2.33 Wm^{-2}) followed by sea salt, black, organic carbon, and sulfate particles (−1.42 Wm^{-2}). The atmospheric heating is proportional to the particle absorptivity. Therefore, the strongest heating (2.33 Wm^{-2}) is caused by black carbon particles, followed by dust (1.72 Wm^{-2}), while the heating effect of the almost purely scattering sea salt and sulfate is small. The non-zero DRE_{atm} of scattering sea salt and sulfate aerosols is possibly related to the increase of the surface backscattered radiation they cause, and therefore the increase of the available radiative energy, which results in an increased absorption by other (absorbing) aerosol types and atmospheric gases above sea salt and sulfate aerosol layers. At TOA, all particles except black carbon cause a cooling effect. The strongest TOA cooling is observed for sea salt and sulfate (−1.23 Wm^{-2} and −0.96 Wm^{-2}, respectively). The DRE_{TOA} caused by organic carbon and dust particles is also negative (however, smaller than the effect of sea salt and sulfate). On the other hand, black carbon particles, despite their relatively small optical depth, cause a substantial TOA heating equal to 0.69 Wm^{-2} due to their strong absorptivity. This depicts the important climatic role of black carbon particles.

Table 2. Annual averaged sulfate aerosol DREs (in Wm^{-2}) for 2015 over: the globe, the Northern and Southern Hemispheres, global land, and ocean areas. The same averages for scattering and absorption AOD at 550 nm are shown in the last two columns.

	DRE_{TOA}	DRE_{atm}	$DRE_{surfnet}$	AOD_{sct}	AOD_{abs}
Global	−0.96	0.46	−1.42	0.036	0.000
Land	−1.46	0.43	−1.90	0.054	0.000
Ocean	−0.73	0.48	−1.21	0.028	0.000
N. Hemisphere	−1.41	0.45	−1.86	0.051	0.000
S. Hemisphere	−0.51	0.48	−0.99	0.021	0.000

Table 3. Annual averaged desert dust aerosol DREs (in Wm^{-2}) for 2015 over: the globe, the Northern and Southern Hemispheres, global land, and ocean areas. The same averages for scattering and absorption AOD at 550 nm are shown in the last two columns.

	DRE_{TOA}	DRE_{atm}	$DRE_{surfnet}$	AOD_{sct}	AOD_{abs}
Global	−0.61	1.72	−2.33	0.028	0.002
Land	−1.24	3.13	−4.36	0.056	0.004
Ocean	−0.33	1.09	−1.41	0.015	0.001
N. Hemisphere	−1.27	2.69	−3.96	0.049	0.004
S. Hemisphere	0.04	0.77	−0.73	0.007	<0.001

Table 4. Annual averaged sea salt aerosol DREs (in Wm^{-2}) for 2015 over: the globe, the Northern and Southern Hemispheres, global land, and ocean areas. The same averages for scattering and absorption AOD at 550 nm are shown in the last two columns.

	DRE_{TOA}	DRE_{atm}	$DRE_{surfnet}$	AOD_{sct}	AOD_{abs}
Global	−1.23	0.59	−1.82	0.042	0.000
Land	−0.14	0.47	−0.61	0.014	0.000
Ocean	−1.73	0.64	−2.37	0.055	0.000
N. Hemisphere	−0.92	0.55	−1.47	0.035	0.000
S. Hemisphere	−1.55	0.63	−2.17	0.049	0.000

Table 5. Annual averaged organic carbon aerosol DREs (in Wm^{-2}) for 2015 over: the globe, the Northern and Southern Hemispheres, global land, and ocean areas. The same averages for scattering and absorption AOD at 550 nm are shown in the last two columns.

	DRE_{TOA}	DRE_{atm}	$DRE_{surfnet}$	AOD_{sct}	AOD_{abs}
Global	−0.72	0.73	−1.45	0.025	<0.001
Land	−1.36	0.87	−2.22	0.039	0.001
Ocean	−0.44	0.66	−1.10	0.018	<0.001
N. Hemisphere	−0.85	0.73	−1.58	0.028	<0.001
S. Hemisphere	−0.60	0.72	−1.33	0.022	<0.001

Table 6. Annual averaged black carbon aerosol DREs (in Wm^{-2}) for 2015 over: the globe, the Northern and Southern Hemispheres, global land, and ocean areas. The same averages for scattering and absorption AOD at 550 nm are shown in the last two columns.

	DRE_{TOA}	DRE_{atm}	$DRE_{surfnet}$	AOD_{sct}	AOD_{abs}
Global	0.69	2.33	−1.64	0.002	0.004
Land	0.97	3.48	−2.51	0.002	0.007
Ocean	0.57	1.81	−1.24	0.001	0.003
N. Hemisphere	0.83	2.78	−1.94	0.002	0.005
S. Hemisphere	0.56	1.90	−1.34	0.001	0.004

4. Conclusions

In this study, MERRA-2 aerosol optical properties and the FORTH deterministic spectral radiative transfer model were used in order to compute the aerosol direct radiative effect (DRE) under clear-sky conditions at the Earth's surface, within the atmosphere, and at the top of the atmosphere (TOA) for 2015 on a global scale. It is found that aerosols cause a cooling of the Earth's surface (−8.73 Wm^{-2}) and a warming of the atmosphere (3.94 Wm^{-2}). These effects were found to be stronger in regions with high aerosol loads, especially consisting of absorbing particles. The aerosol-induced reduction of solar radiation at the Earth's surface contributes to global dimming and is very important for climate because it can reduce the evaporation rates, leading eventually to a slowdown of the water cycle [8,9]. The atmospheric warming caused by aerosols, in

combination with the surface cooling, can result in a stabilization of the atmosphere, and therefore to suppression of cloud formation [10,11], enhancing desertification processes [7]. Overall, aerosols result in a planetary TOA cooling effect above most of the globe, with the exception of a few regions with high surface albedo, such as parts of the Saharan Desert and Greenland, where aerosols cause planetary warming. In general, the aerosol DREs are larger over the Northern than Southern Hemisphere and over land than ocean areas. Profound differences are found between the obtained DREs for different aerosol types. The strongest TOA cooling effect is found for sea salt and sulfate aerosols (−1.23 and −0.96 Wm^{-2}, respectively), while black carbon aerosols cause planetary warming (+0.69 Wm^{-2}). Future work will focus on the determination of long-term DREs as well as the DREs' inter-annual and decadal-scale variations in relation to global dimming and brightening and contribution to climate change.

Author Contributions: Conceptualization, N.H. and A.G.; methodology, N.H., C.M., and A.G.; software, N.H., C.M., and I.V.; formal analysis, M.-B.K.-C. and A.G.; investigation, N.H., C.M., A.G., and M.-B.K.-C.; resources, I.V., N.H., C.M., and A.M.D.S.; data curation, M.-B.K.-C. and A.G.; writing—original draft preparation, M.-B.K.-C. and A.G.; writing—review and editing, N.H.; visualization, M.-B.K.-C.; supervision, N.H. and C.M.; project administration, N.H.; funding acquisition, N.H. All authors have read and agreed to the published version of the manuscript.

Funding: This research was funded by the program "Support for researchers with an emphasis on young researchers—cycle B" of the General Secretariat for Research and Technology-Hellas, grant number 1052.

Institutional Review Board Statement: Not applicable.

Informed Consent Statement: Not applicable.

Data Availability Statement: The data presented in this study are available on request from the corresponding author.

Acknowledgments: The authors acknowledge the Department of Physics of the University of Ioannina, for providing the necessary resources for the performed model computations.

Conflicts of Interest: The authors declare no conflict of interest. The funders had no role in the design of the study; in the collection, analyses, or interpretation of data; in the writing of the manuscript; or in the decision to publish the results.

References

1. Boucher, O.; Randall, D.; Artaxo, P.; Bretherton, C.; Feingold, G.; Forster, P.; Kerminen, V.-M.; Kondo, Y.; Liao, H.; Lohmann, U.; et al. Clouds and Aerosols. In *Climate Change 2013: The Physical Science Basis, Contribution of Working Group I to the Fifth Assessment Report of the Intergovernmental Panel on Climate Change*; Stocker, T.F., Qin, D., Plattner, G.-K., Tignor, M., Allen, S.K., Boschung, J., Nauels, A., Xia, Y., Bex, V., Midgley, P.M., Eds.; Cambridge University Press: Cambridge, UK; New York, NY, USA, 2013; pp. 571–658.
2. Gelaro, R.; McCarty, W.; Suárez, M.J.; Todling, R.; Molod, A.; Takacs, L.; Randles, C.A.; Darmenov, A.; Bosilovich, M.G.; Reichle, R.; et al. The Modern-Era Retrospective Analysis for Research and Applications, Version 2 (MERRA-2). *J. Clim.* **2017**, *30*, 5419–5454.
3. Randles, C.A.; da Silva, A.M.; Buchard, V.; Colarco, P.R.; Dar-menov, A.; Govindaraju, R.; Smirnov, A.; Holben, B.; Ferrare, R.; Hair, J.; et al. The MERRA-2 aerosol reanalysis, 1980 onward. Part I: System description and data assimilation evaluation. *J. Clim.* **2017**, *30*, 6823–6850.
4. Hatzianastassiou, N.; Matsoukas, C.; Drakakis, E.; Stackhouse, P., Jr.; Koepke, P.; Fotiadi, A.; Pavlakis, K.; Vardavas, I. The direct effect of aerosols on solar radiation based on satellite observations, reanalysis datasets, and spectral aerosol optical properties from Global Aerosol Data Set (GADS). *Atmos. Chem. Phys.* **2007**, *7*, 2585–2599.
5. Vardavas, I.; Carver, J.H. Solar and terrestrial parameterizations for radiative convective models. *Planet. Space Sci.* **1984**, *32*, 1307–1325.
6. Korras-Carraca, M.B.; Pappas, V.; Hatzianastassiou, N.; Vardavas, I.; Matsoukas, C. Global vertically resolved aerosol direct radiation effect from three years of CALIOP data using the FORTH radiation transfer model. *Atmos. Res.* **2019**, *224*, 138–156.
7. Hatzianastassiou, N.; Katsoulis, B.; Vardavas, I. Sensitivity analysis of aerosol direct radiative forcing in ultraviolet–visible wavelengths and consequences for the heat budget. *Tellus B* **2004**, *56*, 368–381.
8. Wild, M. Enlightening Global Dimming and Brightening. *Bull. Am. Meteorol. Soc.* **2012**, *93*, 27–37.

9. Hatzianastassiou, N.; Matsoukas, C.; Fotiadi, A.; Stackhouse, P.W., Jr.; Koepke, P.; Pavlakis, K.G.; Vardavas, I. Modelling the direct effect of aerosols in the solar near-infrared on a planetary scale. *Atmos. Chem. Phys.* **2007**, *7*, 3211–3229.
10. Hansen, J.; Sato, M.; Ruedy, R. Radiative forcing and climate response. *J. Geophys. Res.* **1997**, *102*, 6831–6864.
11. Gkikas, A.; Obiso, V.; Pérez García-Pando, C.; Jorba, O.; Hatzianastassiou, N.; Vendrell, L.; Basart, S.; Solomos, S.; Gassó, S.; Baldasano, J.M. Direct radiative effects during intense Mediterranean desert dust outbreaks. *Atmos. Chem. Phys.* **2018**, *18*, 8757–8787.